



## PAPER

# Controlling the photoluminescence of quantum emitters in hexagonal boron nitride by external magnetic fields

RECEIVED  
29 June 2022REVISED  
4 October 2022ACCEPTED FOR PUBLICATION  
13 October 2022PUBLISHED  
28 October 2022

Hilal Korkut and İbrahim Sarpkaya\*

Bilkent University UNAM—National Nanotechnology Research Center, Ankara 06800, Turkey

\* Author to whom any correspondence should be addressed.

E-mail: [sarpkaya@unam.bilkent.edu.tr](mailto:sarpkaya@unam.bilkent.edu.tr)**Keywords:** hexagonal boron nitride, single-photon emitter, magnetic field, defect center, photoluminescence, 2D materialSupplementary material for this article is available [online](#)

## Abstract

The recent observation of room temperature spin-dependent photoluminescence (PL) emission from hexagonal boron nitride's (h-BN's) defect centers motivates for performing a complementary low-temperature photophysical study of quantum emitters under relatively high magnetic fields. Here, we investigate the PL emission dynamics of h-BN's visible single-photon emitters under an applied out-of-plane magnetic field at cryogenic temperatures. The PL intensity of the emitters in our work strikingly exhibits strong magnetic field dependence and decreases with the increased magnetic field. A substantial decrease in the integrated PL intensity of the emitters by up to one order of magnitude was observed when the applied field is increased from 0 T to 7 T. The observed reversible photodarkening of PL emission due to the applied magnetic field is in very well agreement with the predictions of a recent joint experimental and theoretical study and can happen only if the spin-selective, non-radiative, and asymmetric intersystem crossing transitions proceed from the triplet excited state to the lowest-lying spin-singlet metastable state and from the metastable state to the triplet ground state. Our results not only shed more light on the light emission paths of defect centers in h-BN but also show the use of the magnetic field as an efficient control knob in the development of magneto-optical devices.

## 1. Introduction

Hexagonal boron nitride (h-BN) as a wide-bandgap van der Waals material has been considered intensively by the scientific community due to its exciting chemical, optical, electronic, and mechanical properties [1, 2]. It has also attracted much recent interest for the applications of quantum photonics [3] following the first-time demonstration of room-temperature single-photon emission from its defect centers [4]. The exciting properties of h-BN single-photon emitters such as high brightness at room temperature [4], high stability up to 800 K [5], spectral tunability [6–8], large Debye–Waller factor [9], and dipole-like emission with high polarization contrast [10] put them to forefront for those applications. The single photon emitters in h-BN can be activated/created by different post-growth processing techniques including high-temperature annealing, chemical etching, electron beam irradiation, ion

implantation, and laser irradiation [4, 6, 11–13]. The deterministic creation of large arrays of quantum emitters has been also achieved by placing the h-BN onto lithographically patterned silica nano-pillars [14] similar to the deterministic creation of quantum emitters in two-dimensional WSe<sub>2</sub> [15, 16]. The microscopic origin of single-photon emitters emitting in the visible range has been studied extensively and attributed to different types of defects and their complexes [17, 18], whereas the origin of the emitters emitting in the 850 nm region was attributed to negatively charged boron vacancy ( $V_B^-$ ) [19]. The question of whether h-BN has also optically addressable spin defects [20] similar to other wide bandgap materials such as diamond [21, 22] and silicon carbide [23] has been the subject of recent studies and explored in detail. Although early magneto-photoluminescence (PL) studies reported the nonmagnetic behavior of h-BN quantum emitters [9, 24], the spin defects in h-BN materials have been

initialized and readout in optically detected magnetic resonance experiments [19, 25–27] as well as in a recent magneto-PL experiment [28]. The interface between the stationary spin of these defects and the optical photon is not only important for the transfer of quantum information in quantum networks [29, 30] but also for quantum sensing applications [31]. The recent observation of room temperature spin-dependent PL emission from h-BN's defect centers motivates for performing a complementary photophysical study of quantum emitters under relatively high magnetic fields and at low temperatures.

Here, we studied the PL emission dynamics of h-BN single-photon emitters under an applied out-of-plane magnetic field at cryogenic temperatures. Similar to the results of previous experimental studies [9, 24], we did not observe any pronounced Zeeman splitting or shifting of the zero-phonon line (ZPL) emission wavelength. However, the PL intensity of the emitters in our work strikingly exhibits strong magnetic field dependence and decreases with the increased magnetic field. Taking the predictions of a recent joint experimental and theoretical study [28] as a reference, we concluded that the photodarkening of PL emission observed in our work under the applied out-of-plane magnetic field can happen only if the spin-dependent non-radiative intersystem crossing (ISC) transitions happen from the triplet excited state to the lowest-lying spin-singlet metastable state and from the metastable state to the triplet ground state. The results of our low-temperature magneto-PL experiments are very well in agreement with the prediction of [28]. Our results not only shed more light on the light emission paths of defect centers in h-BN but also show the use of the magnetic field as an efficient control knob in the development of magneto-optical devices.

## 2. Methods

### 2.1. Sample preparation and optical characterization at room temperature

In this study, we used commercially available (purchased from 2D Semiconductors company) h-BN flakes in ethanol solution. Before drop-casting the h-BN solution onto a SiO<sub>2</sub>/Si substrate, we cleaned the substrate by using acetone, isopropanol, and distilled water. Following the cleaning process of the substrate, we drop-casted h-BN solution onto the substrate and let it dry overnight under atmospheric conditions. As a next step, the samples were annealed at 850 °C, under 1 Torr argon pressure for 30 min (Protherm Furnace PC 442) to create optically active defect centers. To measure the Raman and PL spectra at room temperature, we used Raman Confocal Microscope (WITec).

### 2.2. Low-temperature PL and magneto-PL measurements

Following its initial optical characterization at room temperature, we further studied the photophysics of those emitters at low temperatures by using the home-built low-temperature micro-PL setup. In that setup, the h-BN samples were mounted inside a closed-cycle cryostat (Attodry 1000) with a base temperature of 3.5 K. The built-in superconducting magnet inside the cryostat was utilized in order to apply magnetic fields in the out-of-plane direction. A picosecond pulsed laser diode operating at 532 nm under both continuous wave (CW) and pulsed mode was used as an excitation source. Following the excitation, emitted PL light was collected via a low-temperature compatible microscope objective (0.82 NA) and coupled to a single-mode fiber after spectrally filtered by a 550 nm long-pass filter. A combination of a 750 mm focal length spectrograph (Princeton Instrument SpectraPro HRS-750) and a liquid nitrogen-cooled silicon charge-coupled device (CCD) camera (PyLoN) was used to record PL spectra. For the second-order photon correlation measurements, emitted PL light was first filtered with a bandpass filter and then directed to the Hanbury Brown and Twiss (HBT) setup consisting of a 50:50 beam splitter connected to two silicon single photon avalanche diode (SPAD) with a photon timing resolution of 50 ps (Micro Photon Devices (MPD)-PDM series). The HydraHarp 400 multichannel picosecond event timer and time-correlated single photon counting (TCSPC) module (PicoQuant) was used in order to obtain coincidence counts. To perform spectral diffusion measurements on the order of 100 ms, the PL emission was directly sent to CCD, whereas it was sent to one of the avalanche photodiodes (APDs) for 1 ms blinking studies.

## 3. Results

### 3.1. Room-temperature optical characterization of h-BN defect centers

In this study, we investigated the photophysics of single-photon emitters in h-BN at low temperatures and under applied out-of-plane magnetic fields. The solution of h-BN containing mono and a few layers of h-BN flakes in ethanol was purchased from the 2D semiconductors company. The thickness of h-BN flakes varies from 1 to 10 atomic layers and 10 nm–10 μm in lateral size. Following the cleaning process of a SiO<sub>2</sub>/Si, a small amount of h-BN solution was drop-casted onto it. To activate defect centers, we applied a thermal annealing process for 30 min at 850 °C under 1 Torr argon pressure. Figure 1(a) shows the optical microscope image of the drop-casted h-BN flakes on the SiO<sub>2</sub>/Si substrate after the thermal annealing process. Figure 1(b) shows the

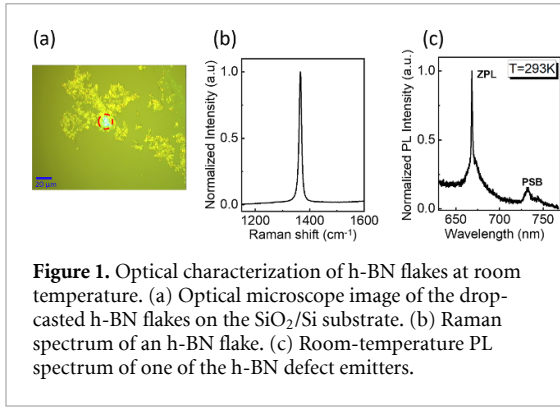


**Figure 1.** Optical characterization of h-BN flakes at room temperature. (a) Optical microscope image of the drop-casted h-BN flakes on the SiO<sub>2</sub>/Si substrate. (b) Raman spectrum of an h-BN flake. (c) Room-temperature PL spectrum of one of the h-BN defect emitters.

Raman spectrum of the h-BN flake taken from the circled region in figure 1(a). The typical Raman shift of thick h-BN flake is given by 1366 cm<sup>-1</sup> (170 meV) and confirms the multilayer nature of the flake [4, 32].

For the PL measurements of defect centers having electronic energy levels inside the band gap of the h-BN, sub-bandgap excitation (532 nm laser) was utilized. Figure 1(c) shows the exemplary room temperature PL spectrum of one of those defect emitters. It consists of a pronounced ZPL located around 668 nm (~1.86 eV) and a low-energy phonon sideband separated from the ZPL by an energy difference of ~160 meV. Similar to the previous studies [6, 9, 33–35], we have also observed PL emissions at different wavelengths spanning the region from 580 nm to 780 nm (supplementary figure 2).

### 3.2. Photophysics of h-BN defect centers at low temperatures

Having confirmed the successful activation of h-BN defect centers, we further probed the emission dynamics of those emitters at liquid helium temperature. For magneto-PL experiments we performed in this work, one needs to have stable and long-term emissions from studied emitters to clearly see the effect of the applied magnetic field. In order to probe the emission dynamics of the h-BN emitters, spectral diffusion and blinking measurements were performed at liquid helium temperature. The top panel of figures 2(a)–(c) shows the low-temperature PL spectra of three different emitters. By sending the PL

emission directly to the silicon CCD camera we recorded the time evolution of the emission with a time resolution of on the order of 100 ms. The central panel of the same figures (d)–(f) shows the corresponding time trajectories of each PL emission which were obtained by continuously integrating the PL spectrum with an integration time of 0.1–0.3 s. To probe the blinking in the PL emission of the h-BN defect emitters in faster time scales, we further increased the resolution of the measurements from 100 ms to 1 ms by sending the emitted light instead to one of the silicon SPADs with a photon timing resolution of 50 ps. Figure 2(g) shows the spectral diffusion (inset of PL plot) and blinking measurements of another h-BN emitter both on the order of 100 ms and 1 ms time scale, respectively. We observed very stable PL emission even at a 1 ms time scale. We measured the PL emission spectra of different emitters at different wavelengths and studied the photostability of those emitters as well. We rarely observed spectral diffusion and blinking (not shown) in the PL emission of those emitters. For our magneto-PL experiments, we eliminated those unstable emitters and worked with the spectral diffusion and blinking free emitters such as in figure 2. Our results evidently show that the emitters in h-BN flakes that we studied provide long-term stable emission, which is essential for both optoelectronic and quantum photonics technologies.

### 3.3. Quantum light emission from h-BN defect centers

To confirm the quantum nature of the emitted light, we have also performed photon antibunching experiments both under CW and pulsed excitation by utilizing an HBT interferometer. Figure 3 shows the histograms of the second-order correlation function for one of the h-BN defect emitters. Observation of pronounced photon antibunching dip in the case of CW excitation (figure 3(b)) or suppressed peak for pulsed excitation (figure 3(c)) at zero delay time with the  $g^2(0)$  values smaller than 0.5 confirms the quantum nature of the emitted light from the studied emitter. In order to obtain the  $g^2(0)$  value in figure 3(b), we used the following equation to fit our data

$$g^2(\tau) = \frac{1 - [1 + a + b] \exp\left(\frac{-|\tau|}{\tau_1}\right) + a \exp\left(\frac{-|\tau|}{\tau_2}\right) + b + \text{bkgr} - 1}{\text{bkgr}}$$

where  $a$  and  $b$  are the background,  $\text{bkgr}$  is the background by uncorrelated light,  $\tau_1$  and  $\tau_2$  are the antibunching constants, and  $\tau$  is the delay time. The obtained  $g^2(0) = 0.27$  value for this particular emitter confirms its quantum nature. The

excited-state lifetime of  $\tau_1 = 3.18$  ns was also obtained for the same emitter. We have performed photon antibunching experiments for different emitters and obtained  $g^2(0)$  values in the range of 0.27–0.40.

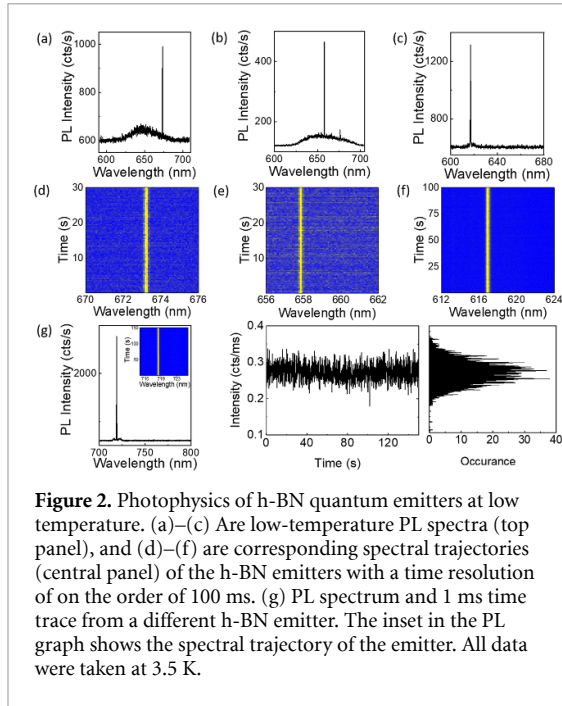


**Figure 2.** Photophysics of h-BN quantum emitters at low temperature. (a)–(c) Are low-temperature PL spectra (top panel), and (d)–(f) are corresponding spectral trajectories (central panel) of the h-BN emitters with a time resolution of on the order of 100 ms. (g) PL spectrum and 1 ms time trace from a different h-BN emitter. The inset in the PL graph shows the spectral trajectory of the emitter. All data were taken at 3.5 K.

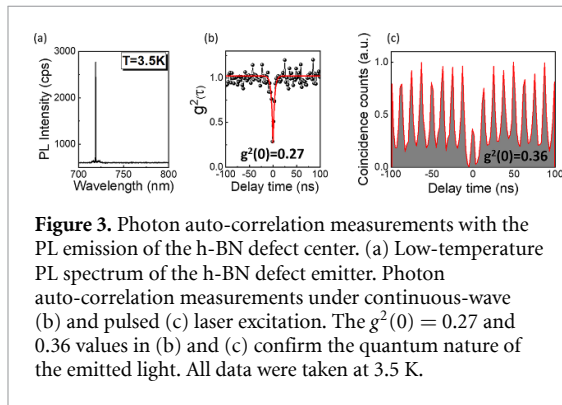


**Figure 3.** Photon auto-correlation measurements with the PL emission of the h-BN defect center. (a) Low-temperature PL spectrum of the h-BN defect emitter. Photon auto-correlation measurements under continuous-wave (b) and pulsed (c) laser excitation. The  $g^2(0) = 0.27$  and  $0.36$  values in (b) and (c) confirm the quantum nature of the emitted light. All data were taken at 3.5 K.

### 3.4. Temperature-dependent PL study of h-BN quantum emitters

To further probe the photophysics of h-BN defect centers, we have performed photon antibunching experiments for another emitter (E8) in a temperature range from 3.5 to 293 K. Figure 4(a) shows the evolution of the ZPL emission in a temperature range from 3.5 to 293 K. The observed redshift (figure 4(b)) in the ZPL energy and broadening of the line width (figure 4(c)) with the increased temperature is a common behavior of localized emitters both in h-BN [24, 33] and other wide bandgap materials such as SiV [36] and chromium defect [37] centers in diamond. As also concluded in one of the previous studies [33], the redshift of the ZPL emission observed in our work can be attributed to the increase in bulk lattice constant whereas the broadening of its line width is attributed to the coupling between the defect center and low-energy acoustic phonons. To confirm the quantum light emission characteristic of this particular emitter in each individual temperature, we have performed second-order

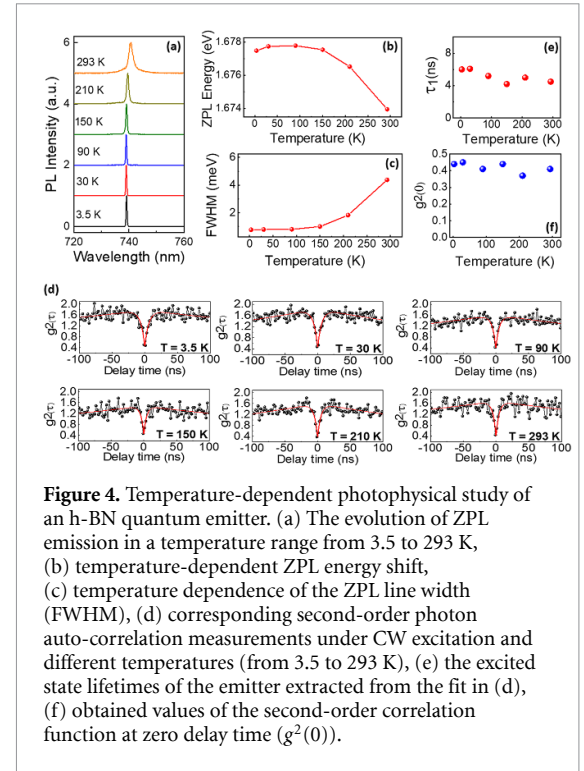
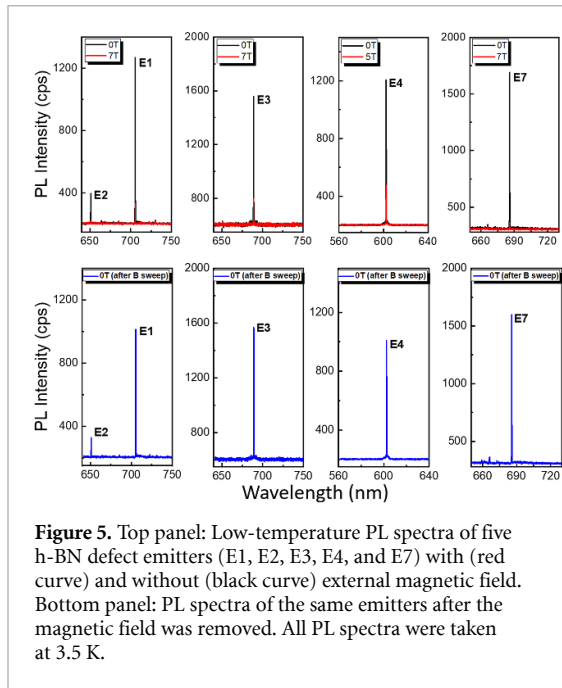


**Figure 4.** Temperature-dependent photophysical study of an h-BN quantum emitter. (a) The evolution of ZPL emission in a temperature range from 3.5 to 293 K, (b) temperature-dependent ZPL energy shift, (c) temperature dependence of the ZPL line width (FWHM), (d) corresponding second-order photon auto-correlation measurements under CW excitation and different temperatures (from 3.5 to 293 K), (e) the excited state lifetimes of the emitter extracted from the fit in (d), (f) obtained values of the second-order correlation function at zero delay time ( $g^2(0)$ ).

photon auto-correlation measurements by sending the PL emission directly to the HBT interferometer. As can be clearly seen from figure 4(d), the emitter sustains its single photon emission behavior at elevated temperatures as well. The data in figure 4(d) have been fitted by utilizing a three-level model and corresponding fitting function. The obtained values of  $g^2(0) = 0.44$  (3.5 K),  $g^2(0) = 0.45$  (30 K),  $g^2(0) = 0.41$  (90 K),  $g^2(0) = 0.44$  (150 K),  $g^2(0) = 0.37$  (210 K), and  $g^2(0) = 0.41$  (293 K) for this particular emitter confirm its quantum nature at corresponding temperatures (figure 4(f)). The excited state lifetimes  $\tau_1$  of the emitter have been also extracted from the fit in (d) and changes between 4.2 and 6 ns (figure 4(e)). They do not show pronounced temperature dependence and are very well in agreement with the observations obtained in the previous studies [24, 33].

### 3.5. Low-temperature magneto-PL studies of h-BN single-photon emitters

Having shown the presence of stable quantum light emitters, we finally studied the behavior of those stable PL emissions under an applied magnetic field in Faraday geometry (e.g. perpendicular to the h-BN plane). The top panel of figure 5 shows the low-temperature PL emission spectra of five different quantum emitters (E) with (red curve) and without (black curve) applied magnetic fields. Similar to the results from the previous experimental studies [9, 24], we did not observe any pronounced Zeeman splitting as well as shifting of the ZPL emission wavelength (supplementary figure 3). However, the PL intensity of the emitters in our work interestingly shows strong magnetic field dependence and decreases with the



increased magnetic field. To rule out the drift-related PL intensity drop under the applied magnetic fields, we maximized the PL intensity each time by adjusting the emitter position with  $x$ ,  $y$ , and  $z$  nanopositioners. We studied eight different emitters and seven of them showed strong magnetic field dependence. Only one of the studied emitters (E6) was not sensitive to the applied magnetic field, and we did not observe any noticeable change in terms of its PL intensity (supplementary figure 4). We also observed that the process is reversible meaning that the PL intensity almost recovers its zero-field value when the applied field is removed. The bottom panel of figure 5 shows the zero-field PL spectrum of each emitter taken just after the magnetic field lowered down to 0 T and confirms the reversibility of the process.

To further illustrate the strong effect of the applied magnetic field on the PL emission of each emitter, in figure 6 we plot the integrated PL intensity of each emitter at different magnetic fields. The integrated PL intensity shows strong magnetic field dependence and decreases with the increased magnetic field. For the E1, E2, and E7, there is an order of magnitude decrease in their integrated PL intensity once the field is increased from 0 T to 7 T. A similar photodarkening effect has also been observed under low magnetic fields for the PL emission of quantum dots (QDs) and was attributed to the trapping of the electrons in a defect-related metastable state acting as a non-radiative decay channel [38]. We also attributed the strong PL intensity drop to the presence of long-lived dark metastable states and analyzed it in detail in the following. We also calculated the integrated PL intensity of E6 under different magnetic fields. As can be seen from the inset of supplementary

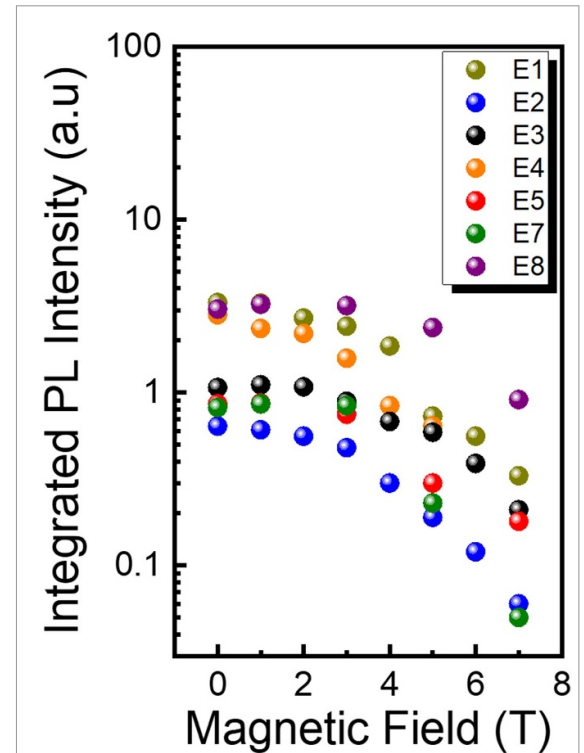


**Figure 6.** Integrated PL intensity of seven h-BN defect emitters as a function of the applied out-of-plane magnetic field. By fitting the PL spectra of each emitter with the Lorentzian function, the area under the PL spectrum is taken as integrated PL intensity.

figure 4, it does not show any pronounced magnetic field dependence and always stays bright. We also note that the reduction of ZPL intensity of h-BN quantum emitters has been also demonstrated in the heterostructure of graphene and h-BN and attributed to the energy transfer from h-BN to graphene [39].

To understand the origin of the strong magnetic field dependence of the PL intensity, we utilized the predictions of the model developed in a recent study [28]. By combining molecular orbital and group theory calculations, Exarhos *et al* proposed different electronic level structures to understand the optical behavior of the visible single-photon emitters of h-BN under the applied in-plane and out-of-plane magnetic fields. The PL simulations of [28] performed according to level diagrams of a defect with a  $C_{2v}$  point group symmetry predict that PL intensity should take its maximum value at  $B = 0$  and decrease strongly with the applied out-of-plane magnetic field if the spin selective, non-radiative, and asymmetric ISC transitions happen from the triplet excited state to the metastable state and from the metastable state to the triplet ground state through the lowest-lying singlet state  $^1A_1$  as shown in the supplementary figure 6. Alternatively, ISC transitions involving both upper ( $^1A_2$  or  $^1B_2$ ) and lower singlet ( $^1A_1$ ) metastable states can also be considered as a possible non-radiative decay paths. The important point in both

cases is that the final ISC transition happens from the lowest-lying  $^1A_1$  state and PL intensity drops when the out-of-plane magnetic field is applied. The results of our low-temperature magneto-PL experiments performed under relatively large out-of-plane magnetic fields are in very well agreement with the prediction of [28] and shed more light on the light emission paths of defect centers in h-BN.

#### 4. Conclusion

In summary, we have studied the PL emission dynamics of h-BN single-photon emitters under an applied out-of-plane magnetic field at cryogenic temperatures. Similar to the results of the early magneto-PL experiments, the ZPL does not show any pronounced Zeeman splitting or shifting of its wavelength. However, the PL intensity of the emitters in our work strikingly shows strong magnetic field dependence and decreases with the increased magnetic field. A substantial decrease in the integrated PL intensity of the emitters by up to one order of magnitude was also observed when the applied field is increased from 0 T to 7 T. Taking the predictions of a recent joint experimental and theoretical study as a reference, we concluded that the photodarkening of PL emission observed in our work under the applied magnetic field can happen only if the spin-selective non-radiative ISC transitions happen from the triplet excited state to the metastable state and from the metastable state to the triplet ground state through the lowest-lying spin-singlet metastable state. Our results not only shed more light on the light emission paths of defect centers in h-BN but also show the use of the magnetic field as an efficient control knob in the development of magneto-optical devices.

#### Data availability statement

The data that support the findings of this study are available upon reasonable request from the authors.

#### Acknowledgments

The authors thank Dr Cüneyt Şahin for the fruitful discussion about the spin selective ISC part of this manuscript. We also thank Dr Wonmi Ahn and Cüneyt Şahin for reading our manuscript and giving valuable feedback. IS acknowledges support from The Scientific and Technological Research Council of Turkey (TÜBİTAK) under the award TÜBİTAK 2232-International Fellowship for Outstanding Researchers (Project No. 118C402) and Tübitak 1001 (Project No. 121F138).

#### ORCID iD

İbrahim Sarpkaya  <https://orcid.org/0000-0002-1181-6174>

#### References

- [1] Caldwell J D, Aharonovich I, Cassabois G, Edgar J H, Gil B and Basov D N 2019 Photonics with hexagonal boron nitride *Nat. Rev. Mater.* **4** 552–67
- [2] Cassabois G, Valvin P and Gil B 2016 Hexagonal boron nitride is an indirect bandgap semiconductor *Nat. Photon.* **10** 262–6
- [3] Turunen M, Brotons-Gisbert M, Dai Y, Wang Y, Scerri E, Bonato C, Jöns K D, Sun Z and Gerardot B D 2022 Quantum photonics with layered 2D materials *Nat. Rev. Phys.* **4** 219–36
- [4] Tran T T, Bray K, Ford M J, Toth M and Aharonovich I 2016 Quantum emission from hexagonal boron nitride monolayers *Nat. Nanotechnol.* **11** 37–41
- [5] Kianinia M, Regan B, Tawfik S A, Tran T T, Ford M J, Aharonovich I and Toth M 2017 Robust solid-state quantum system operating at 800 K *ACS Photonics* **4** 768–73
- [6] Tran T T, Elbadawi C, Totonjian D, Lobo C J, Grosso G, Moon H, Englund D R, Ford M J, Aharonovich I and Toth M 2016 Robust multicolor single photon emission from point defects in hexagonal boron nitride *ACS Nano* **10** 7331–8
- [7] Grosso G, Moon H, Lienhard B, Ali S, Efetov D K, Furchi M M, Jarillo-Herrero P, Ford M J, Aharonovich I and Englund D 2017 Tunable and high-purity room-temperature single-photon emission from atomic defects in hexagonal boron nitride *Nat. Commun.* **8** 1–8
- [8] Noh G, Choi D, Kim J H, Im D G, Kim Y H, Seo H and Lee J 2018 Stark tuning of single-photon emitters in hexagonal boron nitride *Nano Lett.* **18** 4710–5
- [9] Li X, Shepard G D, Cupo A, Camporeale N, Shayan K, Luo Y, Meunier V and Strauf S 2017 Nonmagnetic quantum emitters in boron nitride with ultranarrow and sideband-free emission spectra *ACS Nano* **11** 6652–60
- [10] Jungwirth N R and Fuchs G D 2017 Optical absorption and emission mechanisms of single defects in hexagonal boron nitride *Phys. Rev. Lett.* **119** 1–6
- [11] Chejanovsky N *et al* 2016 Structural attributes and photodynamics of visible spectrum quantum emitters in hexagonal boron nitride *Nano Lett.* **16** 7037–45
- [12] Choi S, Tran T T, Elbadawi C, Lobo C, Wang X, Juodkazis S, Seniutinas G, Toth M and Aharonovich I 2016 Engineering and localization of quantum emitters in large hexagonal boron nitride layers *ACS Appl. Mater. Interfaces* **8** 29642–8
- [13] Hou S, Birowosuto M D, Umar S, Anicet M A, Tay R Y, Coquet P, Tay B K, Wang H and Teo E H T 2018 Localized emission from laser-irradiated defects in 2D hexagonal boron nitride *2D Mater.* **5** 015010
- [14] Proscia N V, Shotan Z, Jayakumar H, Reddy P, Cohen C, Dollar M, Alkauskas A, Doherty M, Meriles C A and Menon V M 2018 Near-deterministic activation of room-temperature quantum emitters in hexagonal boron nitride *Optica* **5** 1128
- [15] Luo Y, Shepard G D, Ardelean J V, Rhodes D A, Kim B, Barmak K, Hone J C and Strauf S 2018 Deterministic coupling of site-controlled quantum emitters in monolayer WSe<sub>2</sub> to plasmonic nanocavities *Nat. Nanotechnol.* **13** 1137–42
- [16] Luo Y, Liu N, Li X, Hone J C and Strauf S 2019 Single photon emission in WSe<sub>2</sub> up 160 K by quantum yield control *2D Mater.* **6** 035017
- [17] Mendelson N *et al* 2021 Identifying carbon as the source of visible single-photon emission from hexagonal boron nitride *Nat. Mater.* **20** 321–8
- [18] Hayee F *et al* 2020 Revealing multiple classes of stable quantum emitters in hexagonal boron nitride with correlated optical and electron microscopy *Nat. Mater.* **19** 534–9
- [19] Gottscholl A *et al* 2020 Initialization and read-out of intrinsic spin defects in a van der Waals crystal at room temperature *Nat. Mater.* **19** 540–5
- [20] Heremans F J, Yale C G and Awschalom D D 2016 Control of spin defects in wide-bandgap semiconductors for quantum technologies *Proc. IEEE* **104** 2009–23

- [21] Doherty M W, Manson N B, Delaney P, Jelezko F, Wrachtrup J and Hollenberg L C L 2013 The nitrogen-vacancy colour centre in diamond *Phys. Rep.* **528** 1–45
- [22] Rose B C *et al* 2018 Observation of an environmentally insensitive solid-state spin defect in diamond *Science* **361** 60–63
- [23] Christle D J, Falk A L, Andrich P, Klimov P V, Hassan J U, Son N T, Janzén E, Ohshima T and Awschalom D D 2015 Isolated electron spins in silicon carbide with millisecond coherence times *Nat. Mater.* **14** 160–3
- [24] Koperski M, Nogajewski K and Potemski M 2018 Single photon emitters in boron nitride: more than a supplementary material *Opt. Commun.* **411** 158–65
- [25] Stern H L *et al* 2022 Room-temperature optically detected magnetic resonance of single defects in hexagonal boron nitride *Nat. Commun.* **13** 1–9
- [26] Chejanovsky N *et al* 2021 Single-spin resonance in a van der Waals embedded paramagnetic defect *Nat. Mater.* **20** 1079–84
- [27] Mu Z *et al* 2022 Excited-state optically detected magnetic resonance of spin defects in hexagonal boron nitride *Phys. Rev. Lett.* **128** 216402
- [28] Exarhos A L, Hopper D A, Patel R N, Doherty M W and Bassett L C 2019 Magnetic-field-dependent quantum emission in hexagonal boron nitride at room temperature *Nat. Commun.* **10** 1–8
- [29] Awschalom D D, Hanson R, Wrachtrup J and Zhou B B 2018 Quantum technologies with optically interfaced solid-state spins *Nat. Photon.* **12** 516–27
- [30] Atatüre M, Englund D, Vamivakas N, Lee S Y and Wrachtrup J 2018 Material platforms for spin-based photonic quantum technologies *Nat. Rev. Mater.* **3** 38–51
- [31] Maze J R *et al* 2008 Nanoscale magnetic sensing with an individual electronic spin in diamond *Nature* **455** 644–7
- [32] Gorbachev R V *et al* 2011 Hunting for monolayer boron nitride: optical and Raman signatures *Small* **7** 465–8
- [33] Jungwirth N R, Calderon B, Ji Y, Spencer M G, Flatté M E and Fuchs G D 2016 Temperature dependence of wavelength selectable zero-phonon emission from single defects in hexagonal boron nitride *Nano Lett.* **16** 6052–7
- [34] Exarhos A L, Hopper D A, Grote R R, Alkauskas A and Bassett L C 2017 Optical signatures of quantum emitters in suspended hexagonal boron nitride *ACS Nano* **11** 3328–36
- [35] Shotan Z, Jayakumar H, Considine C R, Mackoito M, Fedder H, Wrachtrup J, Alkauskas A, Doherty M W, Menon V M and Meriles C A 2016 Photoinduced modification of single-photon emitters in hexagonal boron nitride *ACS Photonics* **3** 2490–6
- [36] Neu E, Hepp C, Hauschild M, Gsell S, Fischer M, Sternschulte H, Steinmüller-Nethl D, Schreck M and Becher C 2013 Low-temperature investigations of single silicon vacancy colour centres in diamond *New J. Phys.* **15** 043005
- [37] Müller T, Aharonovich I, Wang Z, Yuan X, Castelletto S, Prawer S and Atatüre M 2012 Phonon-induced dephasing of chromium color centers in diamond *Phys. Rev. B* **86** 4–9
- [38] Di Vece M, Kolaric B, Baert K, Schweitzer G, Obradovic M, Vallée R A L, Lievens P and Clays K 2009 Controlling the photoluminescence of CdSe/ZnS quantum dots with a magnetic field *Nanotechnology* **20** 135203
- [39] Xu Z-Q, Mendelson N, Scott J A, Li C, Abidi I H, Liu H, Luo Z, Aharonovich I and Toth M 2020 Charge and energy transfer of quantum emitters in 2D heterostructures *2D Mater.* **7** 031001